ADVANCED FUNCTIONAL MATERIALS
www.afm-journal.de



# Effect of Contact Mode on the Electrical Transport and Field-Emission Performance of Individual Boron Nanowires

By *Fei Liu, Zanjia Su, Li Li, Fuyao Mo, Shunyu Jin, Shaozhi Deng, Jun Chen, Chengmin Shen, Hongjun Gao,* and *Ningsheng Xu**

**Vapor–liquid–solid processing of boron nanowires (BNWs) can be carried out either using a bottom-up or top-down growth mode, which results in different contact modes between the nanowire and the substrate. The contact mode may strongly affect the electrical transport and field-emission performance of the individual boron nanowires grown on a Si substrate. The electrical transport and field-emission characteristics of individual boron nanowires of different contact modes are investigated in situ using a scanning electron microscope. The contact barriers are very distinct for the different contact modes. Moreover, the transition from a "contact-limited" to a "bulk-limited" field-emission (FE) process is demonstrated in nanoemitters for the first time, and the proposed improved metal–insulator–vacuum (MIV) model may better illustrate the nonlinear behavior of the Fowler-Nordheim (FN) plots in these nanoscale systems. Individual BNWs with different contact modes have a discrepancy in their emission stability and vacuum breakdown characteristics though they have similar aspect ratios, which suggests that their electrical transport and field-emission performance are closely related to their contact mode. Boron nanowires grown in the base-up mode have better field-emission performances and are more beneficial than those grown in the top-down mode for various device applications.**

## 1. Introduction

Intensive investigations have been carried out on potential device applications using one-dimensional (1D) nanostructures, including carbon nanotubes,[1–3] ZnO nanowires,[4–7] $WO_3$ nanorods,[8,9] AlN nanotips,[10] $TiO_2$ nanotubes,[11] CuO nanobelts, etc.[12] The assembly of these 1D nanostructures into the micro/nanostructure of a device is still considered to be a challenge. The major identifiable problem is whether the results of an assembly process can satisfy the desired device requirements and whether it gives rise to the best performance. Generally, there are two assembly approaches: the bottom-up assembly after growth and the direct growth on micro/nanopatterns prepared by a top-down process. Our approach was concerned with the problem as to what type of contact may exist between the nanowire and the substrate and how this is related to the growth mode. We know that current transport is very much dependent on the contact. Therefore, it is essential to be able to control the direct growth process to give rise to a desirable contact mode. Recently, some researchers have found that the resistance of nanowires can affect their physical properties, such as field emission, piezoelectric, photoelectric-conversion properties, etc.[13–17] It is known that the measured resistance of an individual nanowire essentially consists of three components: the nanowire's intrinsic resistance, the substrate's resistance, and the contact resistance. The contact resistance governs at low-voltage conditions and depends on the applied voltage, so it is rather complicated. Up to date, only a few reports can be found that are concerned with this problem,[13–17] so further systematic studies are necessary.

Boron and boron-based nanomaterials have attracted much attention in recent studies because of their particular properties. Boron nitride nanostructures are usually good insulators with an energy gap of 4.5–5.2 eV, which is much bigger than that of boron nanowires (1.5 eV).[18–20] Accordingly, based on FN theory, boron nitride nanostructures should have a worse FE performance than a boron nanowire. In boron carbonitride (BCN) nanostructures, on the other hand, their conductivity and energy gap often vary with the content of B and N in the graphite network.[21–23] But the controlled doping of uniformly distributed B and N in every nanotube is hard to realize in the fabrication process, which usually leads to variations in emission uniformity in the FE area. Different from other boron-based nanostructures, boron nanowires always

[*] Prof. N. S. Xu, S. Z. Deng, J. Chen, F. Liu, Dr. Z. J. Su, L. Li, F. Y. Mo, S. Y. Jin
State Key Laboratory of Optoelectronic Materials and Technologies, Guangdong Province
Key Laboratory of Display Material and Technology, and School of Physics and Engineering,
Sun Yat-sen University
Guangzhou 510275 (P.R. China)
E-mail: stsxns@mail.sysu.edu.cn
Prof. H. J. Gao, C. M. Shen
Beijing National Laboratory for Condensed Matter Physics, Institute of Physics, Chinese
Academy of Sciences
Beijing 100080 (P.R. China)

DOI: 10.1002/adfm.201000149

exhibit similar and excellent physical properties if they are in the same contact mode, which is slightly affected by other factors. So from the point of actual FE applications, boron nanowires should have a more promising future than boron nitride or BCN nanowires.

In this paper, the effects of the contact mode on the electrical transport and field-emission characteristics of individual single-crystalline boron nanowires (BNWs) with different contact modes are investigated in detail. It is shown that the contact mode is an important factor in determining the field-emission (FE) behavior of nanowires. The physical mechanism underlying the differences in electrical transportation and field emission for the different nanowires is discussed and their FE mechanisms are elaborated on.

## 2. Results and Discussion

Large-area, single-crystalline BNWs were fabricated by thermal reduction and their possible growth mechanism has been reported before in our previous papers.[24,25] Recently, for the purpose of more accurately determining the physical properties of individual boron nanowires, we successfully synthesized BNWs in different density by controlling the growth conditions. The scanning electron microscopy (SEM) images of the as-prepared samples are shown in Figure 1. Figures 1a and 1b are low-magnification images of the BNWs in high density and low density, respectively. The BNWs are distributed on the substrate randomly. Figures 1c and 1d provide the high-resolution images of these nanowires. It can be seen that these BNWs have a mean diameter of about 30 nm and a length of about 5 μm. More importantly, there are typically two kinds of contact modes between the boron nanowire and the substrate as observed in the SEM images of Figure 1c and 1d. The first contact mode is determined by the catalyst being at the bottom of the nanowire, this is the base-growth mode, as shown in Figure 1c. The top of the nanowire is indicated by a white arrow in this image, and no catalyst is observed at its top. By altering the initial preparation conditions, we observed another kind of boron-nanowire growth based on the top-growth mode and in this case the catalyst particle is right at the top of the nanowire, as shown in Figure 1d. The white arrow refers to the location of the catalyst on the boron nanowire. The insets in Figure 1c and 1d respectively provide a schematic showing the base-growth and top-growth modes. It is well known that different growth modes correspond to different contact modes. It has been suggested that the contact mode depends on the strength of the binding force between the catalyst and the silicon substrate at the beginning of the growth.[26]

Our BNWs are single crystals with an α-tetragonal structure, which is the same as those reported in our recent studies.[24,25] Figure 1e is the typical electron-energy loss spectrum (EELS) of a single boron nanowire. The spectrum only shows a peak for boron, no other elements are present, revealing that the as-prepared nanowires are pure BNWs. The catalysts used in our experiments are $Fe_3O_4$ nanoparticles, and a typical transmission electron microscopy (TEM) image is shown in Figure 1f. These catalyst nanoparticles are also single crystals, as can be seen from the corresponding electron-diffraction pattern shown in the inset. The diameter distribution of the nanoparticles is narrow, ranging from 5 nm to 8 nm.

The difference that exists in the electrical-transport and field-emission properties of individual boron nanowires in different contact modes is a question that concerns their use for potential applications. To resolve this question, we have designed a series of measurements that were carried out in a modified high-vacuum SEM system.[9,24] We first compared the electrical-transport properties and the morphological features of base-growth

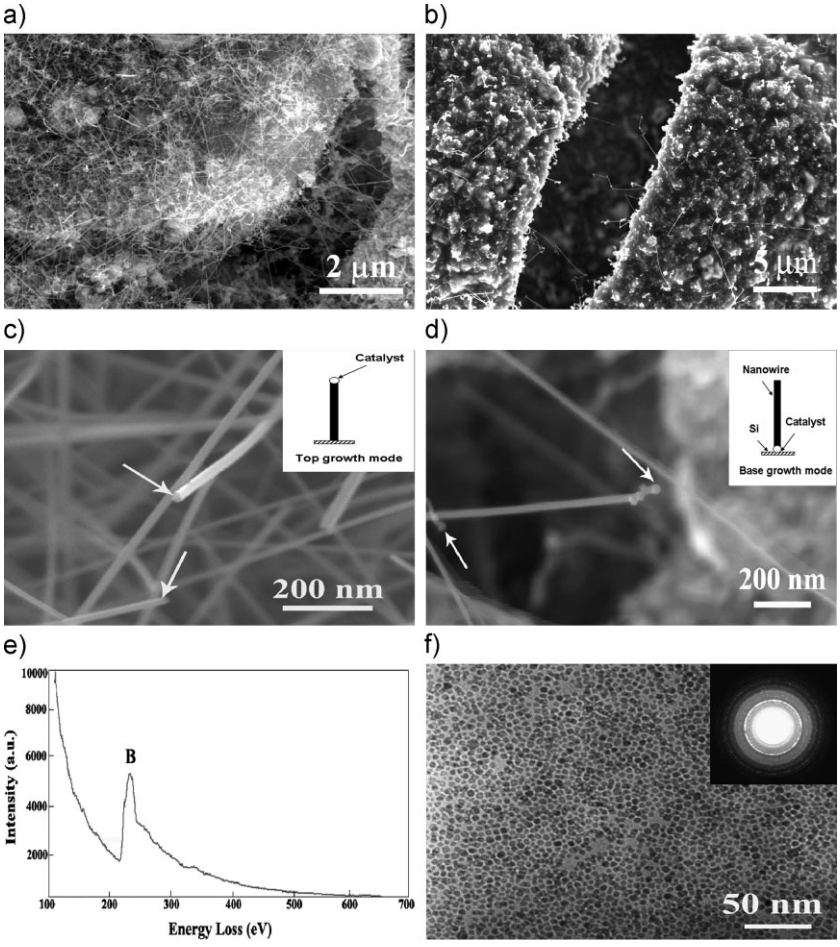


**Figure 1.** a,b) SEM image of high-density and low-density BNWs, respectively. c) Typical SEM image of an individual boron nanowire in base-growth mode. The white arrow indicates the top of the nanowire. d) High-resolution image of an individual boron nanowire in top-growth mode. The end of the nanowire is indicated by the white arrow. The insets in (c) and (d) show the growth mode of the respective nanowires. e) EELS spectrum of a boron nanowire. f) Typical TEM image of $Fe_3O_4$ nanoparticles. The inset shows the corresponding SAED pattern.

individual boron nanowires with those of top-growth individual boron nanowires. For simplicity, we name the base-growth and the top-growth boron nanowires Type-I and Type-II nanostructures, respectively. We chose six individual boron nanowires for comparison and analysis, of which the first three nanowires (I, II, and III) are representative for base-growth nanowires (Type-I) and the other three (IV, V, and VI) are top-growth nanowires (Type-II). The detailed measurement procedure has been described in our previous paper.[24] The SEM images of the measurement procedure are shown in Figure 2. Moreover, in order to eliminate the effect of the catalyst, the W probe was positioned to contact the body of the nanowire. Figures 2a and 2b show the images of the tungsten probe and a single Type-I nanostructure before and during the electrical conductivity measurement. It is obvious that no catalyst exists at the top of this Type-I nanostructure. The SEM images of a single Type-II nanostructure before and during the electrical conductivity measurement are also shown in Figure 2d and 2e. The white arrow indicates the site of the catalyst in this Type-II nanostructure.

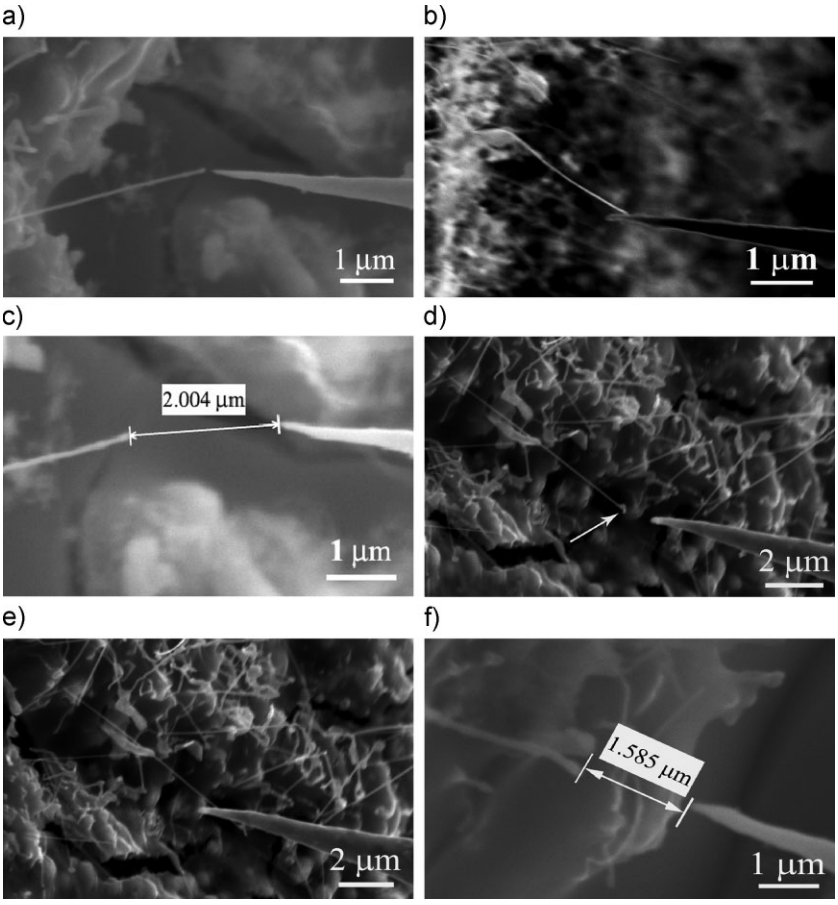


**Figure 2.** a–c) SEM image of the W probe and a single nanowire in base-growth mode (Type-I) a) before the measurement, b) during the electrical conductivity measurement, c) during the field-emission measurement. d–f) SEM image of the W probe and individual nanowire in top-growth mode (Type-II) d) before the measurement, e) during the electrical conductivity measurement, f) during the field-emission measurement.

The total resistance $R_{total}$ in the conductivity experiments should mainly consist of two parts, namely, the contact resistance $R_{Con}$ (energy barrier in transportations) and the intrinsic resistance of the boron nanowire $R_B$. Figure 3a,b shows the electrical conduction ($I$–$V$) curves. It can be seen that the difference between the two types of nanowire is significant. The transitional voltage $V_{critical}$, which is the critical voltage between two divisions in the $I$–$V$ curves, for the individual nanowires in the two contact modes is very different. This critical voltage originates from the variation in the component ratio of their resistances according to our analysis. The intrinsic resistance of individual nanowires can be approximately worked out from the slope of the $I$–$V$ curves in the high-voltage region ($V > V_{critical}$), where their intrinsic resistance dominates in the measured resistance according to the thermal electron field-emission model.[13–16] But when the applied voltage is lower than $V_{critical}$, the contact resistance is predominant in the total resistance. Then it can be concluded that a larger $V_{critical}$ is related to a higher Schottky barrier $\Phi_{sb}$. In general, the intrinsic resistance of a boron nanowire $R_B$ may be expressed as:

$$R_B = \rho_B \frac{l}{s} = \frac{1}{\sigma_B}\frac{l}{s} \Rightarrow \sigma_B = \frac{l}{R_B s} \quad (1)$$

where $\rho_B$ and $\sigma_B$ are the resistivity and conductivity, respectively, of a single boron nanowire, and $l$ and $s$ are the length and cross-sectional area of an individual nanowire.

In order to compare the energy barrier of Type-I nanostructures with that of Type-II nanostructures, the logarithmic plots of the current $I$ as a function of the voltage $V$ are shown in the insets of Figure 3a and b. Based on the thermionic-field emission theory,[13–16] the expression of the current density $J$ in the high-voltage regime ($V > V_{critical}$) can be written as:

$$J(V, \phi_{sb}) = J_{sr}(V, \phi_{sb}) \times \exp\left[V\left(\frac{q}{kT} - \frac{1}{E_0}\right)\right] \quad (2)$$

where $J_{sr}$ slowly varies with the voltage $V$ and is given by

$$J_{sr} = \frac{A^* T (\pi q E_{00})^{\frac{1}{2}}}{k} \exp\left(-\frac{\phi_{sb}}{qE_0}\right) \times \left\{q(V-\zeta) + \frac{\phi_{sb}}{\cosh^2(qE_{00}/kT)}\right\}^{\frac{1}{2}} \quad (3)$$

where $E_{00}$ is a variable parameter in tunnel theory, $\Phi_{sb}$ is the Schottky barrier between the metal and the semiconductor, $E_0$ is

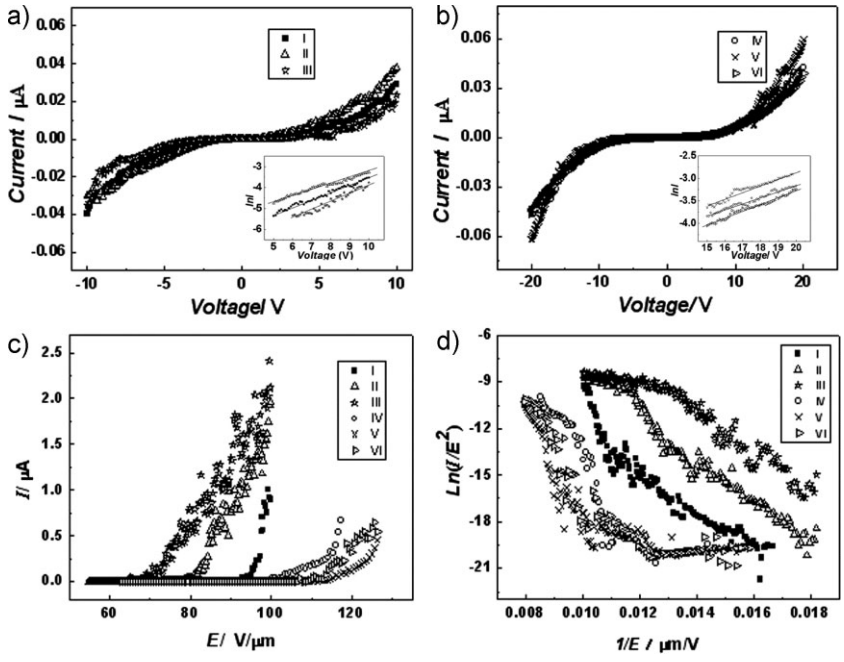


**Figure 3.** a) The *I–V* curves of three individual boron nanowires of Type-I during conductivity measurements. The inset shows their corresponding ln*I–V* curves. b) *I–V* curves of three individual nanowires of Type-II. Their corresponding ln*I–V* curves are shown in the inset. c) *I–E* curves for the six individual BNWs (I–VI) during FE measurements. d) The corresponding FN plots of the curves in (c).

the field at the cathode-vacuum interface, and $\zeta$ is the energy distance between the Fermi level and the conduction level. So the equation for ln$I$ at high voltages ($V > V_{critical}$) can be deduced as:

$$\ln I = \left(\frac{q}{kT} - \frac{1}{E_0}\right) \times V + \ln I_{sr} \quad (4)$$

So the curve of ln$I$ versus $V$ should be linear according to Equation 4. Our observed curves are almost straight lines, revealing that the transportation properties of an individual BNW conform to the thermionic-field emission theory. $E_0$ can be easily obtained by calculating the slope $k$ of the curve of ln$I$ versus $V$, and its average value is 26.3 meV and 26.1 meV for Type-I and Type-II nanostructures, respectively, when the temperature $T$ of the nanowire is 297 K. The $E_0$ values for both contact modes are very similar, which indicates that the electric field between the nanostructure and the probe is not the determinant factor in the measurements. Commonly, the extrapolation of the ln$I$–$V$ curves (0, ln$I_{sr}$) on the ln$I$ axis intensively depends on the height of the Schottky barrier $\Phi_{sb}$, that is, a larger $|\ln I_{sr}|$ value corresponds to a higher Schottky barrier. These experimental results are summarized in Table 1. Through detailed comparisons, it was first found that the energy barrier of Type-II nanostructures is generally higher than that of Type-I nanostructures because these nanowires have larger $V_{critical}$ and $|\ln I_{sr}|$ values. Secondly, the intrinsic conductivity of the individual boron nanowires was very similar (ca. $2.9 \times 10^{-2}$ $\Omega^{-1}$cm$^{-1}$) independent of their contact mode (Table 1), which suggests that the contact mode may play a more important role in determining the transportation properties in comparison to its effect on their morphological features.

To understand the effect of the contact mode on the nanowire's electrical transportation process, we proposed band diagrams for boron nanowires grown in the different contact modes, as shown in Figure 4a,b. Here, iron nanoparticles are thought to be the actual catalysts existing on the nanowire because the $Fe_3O_4$ nanoparticles used in the growth process are usually reduced to Fe nanoparticles at high temperature ($T$ >900 °C) in $H_2$ atmosphere according to our observations and some previous literature.[27,28] As seen in Figure 4, the nanowires in the two contact modes have different band diagrams for their conductivity measurements. For Type-I nanostructures, the first contact barrier results from double hetero-junction barriers between the n-type heavily doped silicon substrate and the boron nanowire, and the second barrier is related to the contact resistance between the nanowire and the tungsten probe. The first contact barrier of Type-I nanostructures consists of two Schottky barriers, where one is the resistance between the Fe catalyst and the n-type heavily doped silicon substrate and the other comes from the resistance between the Fe catalyst and the boron nanowire. But when we consider that the many surface or defect states existing on the surface of the individual nanowire pin the Fermi level and that the Fe catalyst particles located at the interface induce a doping-level in the energy gap of the silicon substrate, the height of these two Schottky barriers should be decreased to a very low extent for Type-I nanostructures. Moreover, the barrier depth ($qV_{D3}$) of the second contact barrier can be ignored for both Type-I and Type-II nanostructures because the work function of the W probe is nearly

**Table 1.** List of morphological parameters, contact mode, and conductivity for different individual BNWs.

| Sample number | Growth mode | Length [μm] | Diameter [nm] | Intrinsic conductivity $\sigma_B$ [$\Omega^{-1}$cm$^{-1}$] | $E_0$ [meV] | $\lvert\ln I_{sr}\rvert$ (reflects on Schottky barrier) | Average $V_{critical}$ [V] |
|---|---|---|---|---|---|---|---|
| I | Base-growth | 4.8 | 25 | $3.1 \times 10^{-2}$ | 26.3 | 6.961 | |
| II | Base-growth | 5.1 | 30 | $2.9 \times 10^{-2}$ | 26.2 | 7.173 | 5.6 |
| III | Base-growth | 5.3 | 35 | $2.85 \times 10^{-2}$ | 26.3 | 7.895 | |
| IV | Top-growth | 5.0 | 30 | $2.9 \times 10^{-2}$ | 26.1 | 5.871 | |
| V | Top-growth | 4.8 | 25 | $3.1 \times 10^{-2}$ | 26.1 | 6.292 | 13.1 |
| VI | Top-growth | 5.3 | 35 | $2.85 \times 10^{-2}$ | 26.1 | 6.067 | |

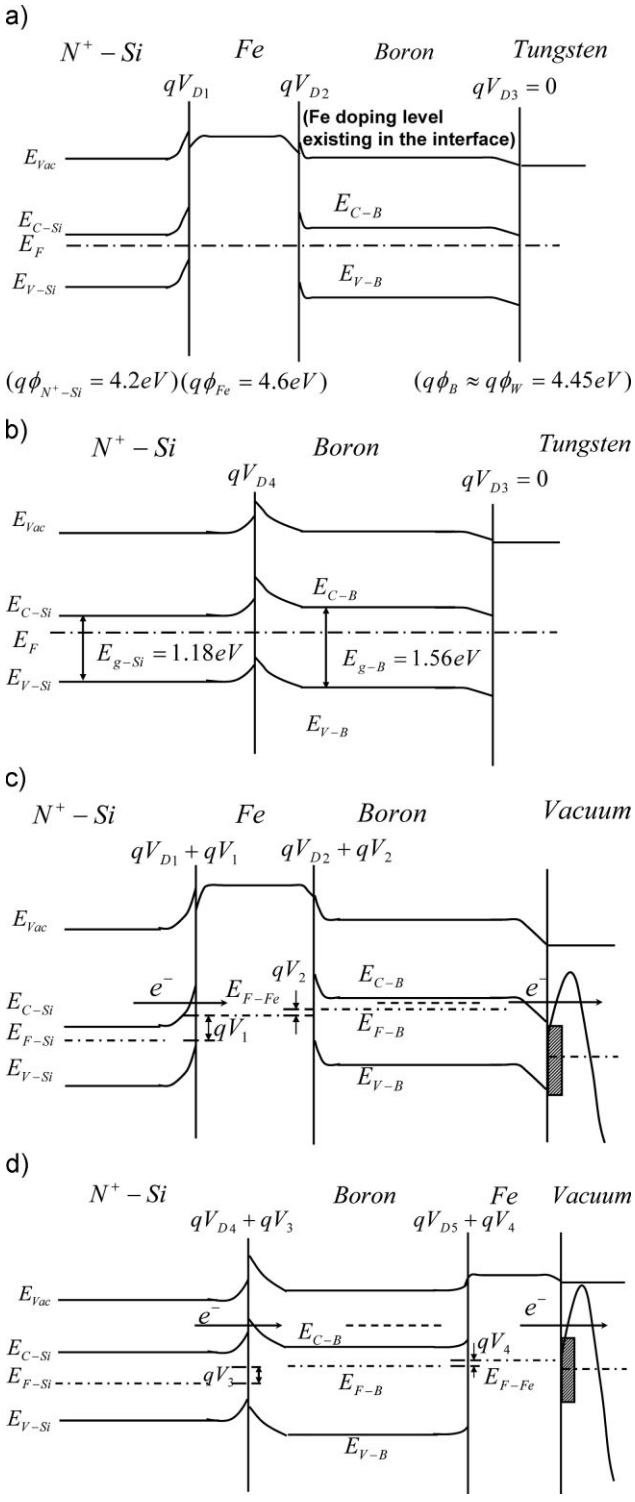


**Figure 4.** a,b) Band diagrams of individual boron nanowires in conductivity measurements for a) Type-I and b) Type-II BNWs. c,d) Their corresponding band diagrams in field-emission measurements for c) Type-I and d) Type-II BNWs.

equal to that of the boron nanowire. For Type-II nanostructures, the contact resistance is a hetero-junction barrier between the boron nanowire and the n-type heavily-doped Si substrate. Considering the effect of the surface states on hetero-junctions, the surface levels of the silicon substrate and the boron nanowire are all elevated to form a first contact barrier ($qV_{D4}$). Analyzing the above-mentioned band diagrams, it is reasonable to assume that a lower contact barrier ($qV_{D1}+qV_2<qV_{D4}$) exists in Type-I nanostructures, and thus a larger current should go through the barrier when the same electric field is applied to the different types of individual nanowires, which is consistent with our experimental curves (Fig. 3). It suggests that the conductivity measurements of individual boron nanowires are mainly affected by the first contact resistance in their hetero-junction structures.

We further explore how the contact mode affects the field-emission process of an individual nanowire. The SEM images of individual Type-I and Type-II boron nanostructures during field-emission measurements are shown in Figure 2c and 2f. The distance between the individual nanowire and the W probe in the experiment was usually 1.5 μm for all measurements. The field-emission current versus electric field ($I$–$E$) curves and their corresponding FN plots are given in Figures 3c and 3d, respectively. Table 2 compares the above parameters for both types of individual nanowires. Firstly, it is found that the emission current of Type-I nanostructures exhibits a much faster increase with increasing applied voltage than that of Type-II nanostructures. Secondly, it can be seen that the individual nanowires with the same contact mode show similar FE behavior. Thirdly, it can be observed that individual Type-I nanostructures have a larger emission-enhancement factor ($\beta$) than Type-II nanostructures. Earlier, Bai and coworkers showed that a nanowire with a catalyst particle on the emitting tip has a better field-emission performance as the existence of a catalyst particle induces a lower work function.[21] According to Bai's suggestions, Type-II nanostructures should possess a better FE performance than their Type-I counterparts, because Type-II nanostructures have a catalyst particle on their tips. However, in our measurements, we did not see evidence of this effect on our Type-II nanostructures because the work function of Fe (4.6 eV) is very close to that of boron (4.45 eV), which also further suggests that the contact mode is a more significant factor in determining the individual nanowire's FE properties in comparison with the presence or absence of a catalyst particle on the tip.

In order to understand the field-emission characteristics observed, we examined whether conventional FN theory is applicable to our nanowires. The classical FN equation is expressed as:[29]

$$J = A\left(\frac{\beta^2 E^2}{\phi}\right)\exp\left(\frac{-B\phi^{\frac{3}{2}}}{\beta E}\right) \tag{5a}$$

and FN plots are generally derived as:

$$\ln\left(\frac{J}{E^2}\right) = -\frac{B\phi^{\frac{3}{2}}}{\beta}\cdot\frac{1}{E} + \ln\frac{\beta^2}{A\phi} \tag{5b}$$

where $A = 1.57\times10^{-10}$ ($AV^{-2}eV$), $B = 6.83\times10^{9}$ ($Vm^{-1}eV^{-3/2}$), $E$ is the applied vacuum gap field, $J$ is the field-emission current

**Table 2.** Detailed field-emission behavior for single BNWs in different contact modes.

| Sample | | Aspect ratio | Operation voltage at 1 nA [V] | Electrical voltage at 500 nA [V] | $\beta_l$ (at low voltage <90 V) | $\beta_h$ (at high voltage >90 V) | Breakdown voltage [V] | Emission Instability |
|---|---|---|---|---|---|---|---|---|
| Base-Growth (Type I) | I | 192 | 100.29 | 128.4 | 2800 | 3200 | | |
| | II | 170 | 87.2 | 116.1 | 3600 | 4100 | 423 | <22% |
| | III | 151 | 118.58 | 145.95 | 2700 | 2280 | | |
| Top-Growth (Type II) | IV | 167 | 154.25 | 183.75 | 2200 | 480 | | |
| | V | 192 | 142.91 | 174.6 | 2400 | 520 | 236.4 | <40% |
| | VI | 151 | 158.99 | – | 2100 | 550 | | |

density, and $\phi$ is the work function of a single boron nanowire (established as being 4.4 eV from our previous results).[24] The enhancement factor $\beta$ is inherently related to the morphological characteristics of the emitter and can be approximately described as:[30]

$$\beta = \frac{(\lambda^2 - 1)^{1.5}}{\lambda \ln\left[\lambda + (\lambda^2 - 1)^{\frac{1}{2}}\right] - (\lambda^2 - 1)^{\frac{1}{2}}} \tag{6}$$

where $\lambda = l/r$ is the aspect ratio of the nanowire, that is, its length divided by its radius. Based on this theory, individual nanowires having similar $r$ and $l$ values should possess similar $\beta$ values, and their FN plots should be linear. However, it can be seen in Figure 3d that the FN plots of both Type-I nanostructures and Type-II nanostructures are divided into two regions, namely, a high-current region and a low-current region, and that their $\beta$ values are very distinct. Thus, conventional FN theory cannot be used directly to explain our experimental results. On the other hand, our electrical-transportation measurements show that the individual boron nanowires exhibit visible semiconductor characteristics. This observation and the nonlinear behavior of the FN plots led us to improving the original metal–insulator–vacuum (MIV) model, which was developed by Bayliss, Latham, and Xu.[31]

An improved MIV field-emission mechanism can be described as follows. The band diagrams of our double hetero-junctions are shown in Figure 4c and d to better illustrate the whole emission procedure of our individual boron nanowires with different contact modes. It can be seen that an energy barrier exists between the individual boron nanowire and the silicon substrate when no field is applied and there is a notable difference between the two contact modes. When the vacuum gap field is applied, the energy barrier becomes narrower and quantum tunneling occurs. The band diagrams show an evident discrepancy for the depth of the energy barrier for electron emission for the different kinds of nanowire and the contact resistance of Type-II nanostructures is still larger than that of Type-I nanostructures in the high negative-voltage regions. As discussed by Latham and Xu,[31] the initial rapid increase of the emission current at low fields results from electron injection at the interface between the substrate and the nanowire. This process is called "contact-limited" because most of the applied voltage falls across the contact resistance. In this stage, the intrinsic resistance $R_B$ of the boron nanowire is much smaller than the contact resistance $R_{Con}$. Simmons derived the characteristic expression of the tunnel current through the hetero-junction for the MIV model as follows:[32,33]

$$j_T = \frac{5.56 \times 10^{-14}}{\varepsilon^* q V_D} N_D (V_C + \phi_m - \phi_I) \exp\left[-3.6 \times 10^{13} \left(\frac{(qV_D)^3 \varepsilon^*}{N_D (V_C + \phi_m - \phi_I)}\right)^{\frac{1}{2}}\right] \tag{7}$$

For our case, $\phi_m$ and $\phi_I$ are respectively the work functions of Fe ($\phi_{Fe} = 4.6$ eV) and for the n-type heavily doped silicon substrate ($\phi_{Si} = 4.2$ eV) or for the boron nanowire ($\phi_B = 4.45$ eV), $qV_D$ is the contact-barrier height between Fe and the semiconductor (n-type heavily doped Si or boron), $\varepsilon^*$ is the dielectric constant of silicon or boron, $N_D$ is the donor density of silicon or boron, and $V_C$ is the potential appearing across the barrier. This equation shows a tendency of a sharply rising current dependence with applied voltage, and a rapid falling of the contact resistance $R_{Con}$. The contact-limited conduction will continue until the contact resistance $R_{Con}$ is equal to the boron nanowire's intrinsic resistance $R_B$ at a particular voltage. After which, $R_{Con}$ is always lower than $R_B$. So when the applied voltage keeps increasing, "bulk-limited" conduction will become dominant, which means that the applied voltage will mainly fall in the boron nanowire at this stage. The $J$–$V$ relationship for bulk-limited conduction is expressed as:[33]

$$j = j_0 \exp\left[\frac{e}{kT}\left(\frac{eV_B}{\pi\varepsilon\varepsilon_0 l}\right)^{\frac{1}{2}}\right] \text{ or } j = j_0 \exp\left[\frac{e}{2kT}\left(\frac{eV_B}{\pi\varepsilon\varepsilon_0 l}\right)^{\frac{1}{2}}\right] \tag{8}$$

where $V_B$ is the voltage appearing at the boron nanowire, $\varepsilon_0$ and $\varepsilon$ are respectively the dielectric constant of free space and the relative dielectric constant of boron, $l$ is the length of the boron nanowire, and $j_0$ is the current density at low field. As a result, the sharp increase of current density with increasing applied field ceases, in other words, the increasing tendency of the field-emission current with the applied field slows down. Thus, a transition from "contact-limited" to "bulk-limited" conduction takes place in our field-emission experiments as we observed in the FE curves. Based on the improved MIV model, the $J$–$E$ curve of individual BNWs should be clearly divided into two regions, corresponding to a contact-limited region and a bulk-limited region, because of the different current equations existing for these two different emission processes. Accordingly, the FN curve

for individual boron nanowires should also be separated into two linear regions for the different emission processes, which is consistent with our experimental curves, as seen in Figure 3d. It can be concluded that our improved MIV theory can be successfully used to illustrate the emission behavior for individual boron nanowire in the same contact mode. In addition, the transition from "contact-limited" conduction to "bulk-limited" conduction was observed for the first time both in the *I–E* curves and in the FN plots for our nanoscale systems, which may provide new ideas for illustrating the nonlinear behavior of nanomaterials in field-emission devices.

However, a fact that still needs to be explained is the different FE performance for individual nanowires in the different contact modes. When an equally high voltage is applied between the W probe and the individual nanowire, the total fallen voltage $V$ will appear both in $R_B$ and $R_{Con}$, and $V$ can then be expressed as $V = V_{Con} + V_B$. The effective voltage $V_B$ on the individual nanowire will be different depending on the contact mode because the contact mode leads to a different contact resistance in the Type-I and Type-II nanostructures. In parallel with our discussion on the conductivity in the nanowires for both contact modes, it is clear that the falling of $V_B$ in Type-I nanostructures will be higher than that in Type-II nanostructures because the lower applied voltage $V_{Con}$ is wasted over the contact resistance $R_{Con}$ for Type-I nanostructures. Hence, a higher $V_B$ ensures a better emission performance for Type-I nanostructures than for Type-II nanostructures, as shown in Table 2. It is evident that the field-emission behavior of sample II is the best (the operation voltage at 1 nA is 87.2 V) and that of sample VI is the worst (operation voltage at 1 nA is 158.99 V) for our six individual boron nanowires, which conforms well to our analysis on their contact resistance. As seen in Figure 3d, the profile of $\ln(I/V^2)$ versus $1/V$ plots is different for Type-I and Type-II nanostructures. For Type-II nanostructures, a larger $\beta$ value is found at low electric fields than at high electric fields, which is different from Type-I nanostructures. This is probably related to the fact that a different order of magnitude in the contact resistance $R_{Con}$ is found for the different contact modes resulting in different current compositions depending on the field strength. This leads to a difference in shape of the FN plots between the high field and low field. Whereas for the same contact mode, the same tendency in the *I–E* curves and FN plots are found, which further proves that the contact mode has a great effect on the field-emission properties of a single boron nanowire. A small difference in FN plots for the same contact mode of individual boron nanowires can also be observed because some difference still exists in the contact resistance for different nanowires, which comes from the alloying degree between the Fe catalyst and the silicon substrate.

Consequently, we examines how the contact mode affects the high emission current capacity of boron nanowires. We designed some experiments to measure the field-emission breakdown properties of these two kinds of boron nanowire. Figure 5a shows a typical *I–V* curve of a Type-I nanostructure recorded in a breakdown procedure. It may be divided into three steps, corresponding to the SEM images of Figure 5b–d. The white

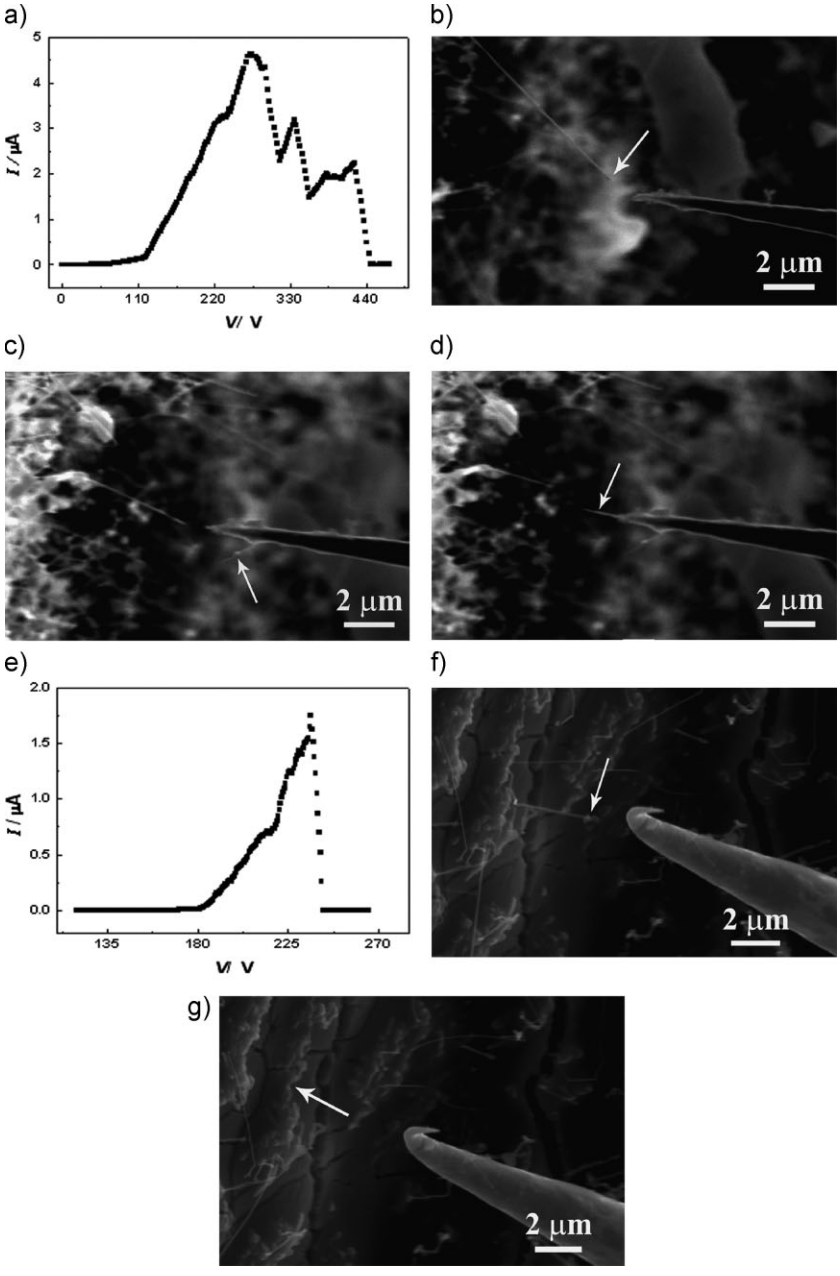


**Figure 5.** a) Typical breakdown curve of Type-I nanostructures. b–d) SEM images of a three-step breakdown procedure for an individual Type-I boron nanostructure. e) The typical breakdown curve of a Type-II nanostructure. f,g) SEM images of an individual Type-II boron nanostructure before and after the breakdown procedures, respectively.

arrow shows the location of the nanowire. When the applied voltage was increased to a set value (about 300 V), part of the nanowire broke off and got stuck on one side of the probe because of the applied electrical field, as shown in Figure 5c (see white arrow). Further increasing of the applied voltage resulted in another part of the nanowire to be broken off and attached to another side of the tungsten probe, as shown in Figure 5d. The possible breakdown procedure can be depicted as follows. The field-emission current may cause Joule heating to occur in the emitter, and localized regions with a higher resistance, because of crystal defects that have been shown to occur in these individual boron nanowires, can experience very high temperatures because of the higher Joule heating.[25,32,34] So when a high voltage is applied to the nanowire, regions with a high density of defect sites will reach higher temperatures and melt first, leading to a breakage in the nanowire. It can also be seen from Figure 5a that the emission current decreases after each break and that the peak emission is lower each time. This can be explained as follows. The distance between the probe and the nanowire is larger after each break and consequently the effective field is smaller. The maximum current is lower for each consecutive emission because the length of the nanowire becomes shorter after each break. This process is repeated until the nanowire was completely destroyed.

Figure 5e shows the representative *I–V* curve of an individual Type-II nanowire. It is very clear that this is different from that of a Type-I boron nanostructure. From the curve and the corresponding SEM images (Fig. 5f,g), only one breakdown process can be found. The white arrow in Figure 5f shows the catalyst at the top of the nanowire, which proves that the nanowire belongs to Type-II. The broken region was located at the contact site between the nanowire and the substrate, indicated by the white arrow in Figure 5g. For Type-II nanostructures, $R_{Con}$ is higher than the resistance of any localized regions in the nanowire based on the band diagram in Figure 3d. So when a high voltage is applied to the sample, the contact site has the highest resistance and will thus reach the highest temperature first. The breakdown thus occurs at the contact point between the nanowire and the substrate and the emission current will immediately decrease to zero, which agrees with the breakdown curve in Figure 5e. The detailed breakdown data are recorded in Table 2. From this table, it can be seen that Type-I nanostructures have a higher breakdown voltage (about 423 V) than Type-II nanostructures (about 236.4 V). Moreover, it is also found that Type-I nanostructures can endure higher currents (about 5 μA) than Type-II nanostructures (about 2 μA), which also further testifies our improved MIV model. It can thus be concluded that Type-I nanostructures, namely nanowires grown from the base-up, seem to be better both from the point of endurance to high currents or from their breakdown properties.

The tip of the nanostructure has also been reported to affect the physical properties, a point that should also be considered for these individual boron nanowires. There are usually two factors concerning the effect of the tip structure on CNTs.[35–41] One is that the field-enhancement factor will vary with the actual shape and size of the tip, which is not necessarily spherical.[35–37] For instance, if the radius of one nanowire is 5 times larger than that of another nanowire, its enhancement factor is reported to be 2 times larger than that of the other nanotube. Another factor is the geometry configuration of the CNT on the tip, which can induce a variation in the electron states and can decrease their work function.[38–41] This factor is more significant than the shape factor as has been reported in recent studies.[38,41] In our experiments, the tip radius of the individual boron nanowires was considered to have the radius of a hemisphere. Our selected individual nanowires had similar diameters and tip shapes as deducted from SEM images, so the shape effect on the field-enhancement factor should be much lower than that of the contact mode. Moreover, unlike individual carbon nanotubes, the tips of our individual boron nanowires should possess similar work functions for nanowires of the same contact mode because they are perfect single-crystalline nanowires with the same covalent bonds. Thus, it can be concluded that the contact mode plays a key role in determining the FE properties of individual boron nanowires in comparison with other possible influencing factors.

Finally, the emission stability of the nanowires of different contact modes were investigated, which was crucial for evaluating the effect of the contact mode on cathode nanomaterials. Technologically speaking, the stability at high working currents is more valuable than that at low currents. Figure 6 shows the representative emission stability curves at high emission currents. The measurements were conducted for the duration of one hour. The applied electrical voltage was respectively fixed at 135 and 180 V for Type-I and Type-II nanostructures, and the adopted emission current was 0.5 μA at the beginning of the measurements. It can be observed that individual nanowires with the same contact mode have almost identical field-emission stability performances. Moreover, it is evident that individual Type-I boron nanostructures exhibit a more stable field emission at high current (less than22% variation in the current) than Type-II nanostructures (less than 40%) throughout the whole emission operation. Because $R_{Con}$ changes with increasing applied field, based on our improved MIV model, it will introduce some fluctuations in the emission current during the stability measurements. Type-II nanostructure possess higher $R_{Con}$ values than Type-I nanostructures, so their field-emission stability behavior is expected to be worse than that of Type-I nanostructures, which is in good agreement with the observed results in Figure 6. Some other factors that may influence the emission stability have been published before in a previous

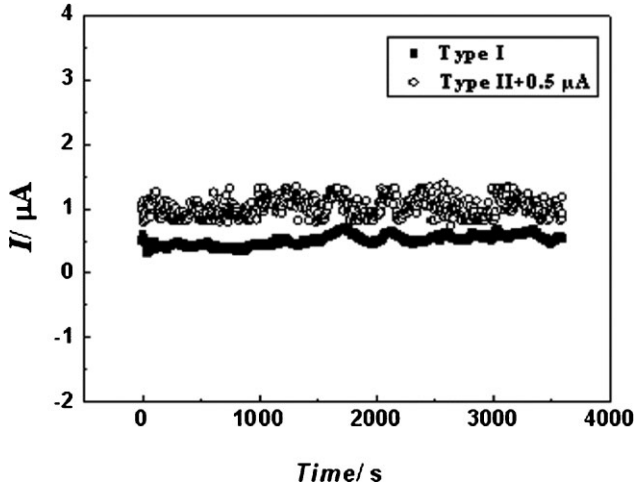


**Figure 6.** Representative emission stability curves of the different contact modes of individual boron nanowires at high current (0.5 μA).

paper.[24] Even if there is some degree of instable emission existing in these individual nanowires at high current, they are still acceptable enough for field-emission devices because the emission current of these individual boron nanowires is far lower than 0.5 μA in practical applications. Through our comparisons of Type-I and Type-II nanostructures for many field-emission characteristics, we can conclude that the contact mode is a more essential factor in determining the emission properties of individual nanowires than their intrinsic conductivity or morphological features. So in order to control the uniform physical properties of these nanowires and effectively improve their properties to be suitable for various applications, only nanowires that have been grown from the base-up should be used to fabricate devices. At present we are still making progress in controlling the growth mode of uniform BNWs, and further research is still undergoing.

## 3. Conclusions

The field-emission behavior of individual BNWs in different contact modes was compared in detail. It was found that the height of the contact barrier of individual Type-I nanostructures (base-growth mode) is distinctly higher than that of Type-II nanostructures (top-growth mode), which results from the discrepancy of the contact modes between the nanowire and the substrate. It was also found that the intrinsic conductivity of individual nanowires with different contact modes is very close, suggesting that the contact mode strongly affects the FE performance (operation field, breakdown field, and stable emission) of a single nanowire. It is worthy of noting that the transition mechanism of "contact-limited" conduction to "bulk-limited" conduction could be applied to explain the two-stage behavior of the *I–E* curves and nonlinear behavior of the FN plots in our nanoscale systems. In addition, according to our investigations on individual boron nanowires in different contact modes, we can conclude that for practical applications in devices the controlled synthesis of nanowires in the base-growth mode is imperative.

## 4. Experimental

Boron nanowires in different densities were successfully fabricated by a thermal carbon-reduction method in a single-stage furnace developed in our group [42,43]. A high-temperature solution phase reaction was used to synthesize the $Fe_3O_4$ nanoparticle catalysts [44,45]. The mass ratio of boron powder, boron oxide powder, and carbon powder was adjusted to obtain different densities of nanowires. In the whole reaction process, the flow rate of Ar gas to $H_2$ gas was controlled to be 300:10 sccm and the pressure in the chamber was kept at $10^5$ Pa. The furnace was ramped to 1000–1100 °C at a rate of 20 °C $min^{-1}$ and held at that temperature for 2–4 h. After cooling to room temperature, the products were collected on a Si[001] substrate.

The morphologies of the BNWs were investigated on a field-emission type scanning electron microscope (XL-SFEG, FEI Corp.). A high-resolution transmission electron microscope (Tecnai F20, FEI Corp.) equipped with an electron-energy loss spectroscope was used to obtain the EELS spectrum of the BNWs and the crystalline structures of the $Fe_3O_4$ nanoparticles. The field-emission (FE) properties of the individual BNWs were tested using a modified SEM system (JEOL-6380) [9].

## Acknowledgements

This work was supported by the National Basic Research Program of China (973 Program, Grant No. 2007CB935500, 863 Program, Grant No. 2007AA03Z305, Science foundation for young scholars, Grant No. 50802117), the National Joint Science Fund of the Guangdong Province (Grant No. U0634002, U0734003), the Foundation of Education Ministry of China (Grant No. 20070558063, 09lgpy28), the Science and Technology Department of Guangdong Province, the Education Department of Guangdong Province, and the Science and Technology Department of Guangzhou City.

Received: January 26, 2010
Revised: March 8, 2010
Published online: May 11, 2010

[1] B. Liu, M. A. McCarthy, Y. K. Yoon, D. Y. Kim, Z. C. Wu, F. So, P. H. Holloway, J. R. Reynolds, J. Guo, A. G. Rinzler, *Adv. Mater.* **2008**, *20*, 3605.
[2] W. B. Choi, D. S. Chung, J. H. Kang, H. Y. Kim, Y. W. Jin, I. T. Han, Y. H. Lee, J. E. Jung, N. S. Lee, G. S. Park, J. M. Kim, *Appl. Phys. Lett.* **1999**, *75*, 3129.
[3] J. F. Wu, M. Wyse, D. McClain, N. Thomas, J. Jiao, *Nano Lett.* **2009**, *9*, 595.
[4] H. H. Huang, G. J. Fang, X. M. Mo, L. Y. Yuan, H. Zhou, M. J. Wang, H. B. Xiao, X. Z. Zhao, *Appl. Phys. Lett.* **2009**, *94*, 063 512.
[5] J. Y. Son, S. J. Lim, J. H. Cho, W. K. Seong, H. J. Kim, *Appl. Phys. Lett.* **2008**, *93*, 053 109.
[6] X. D. Wang, J. H. Song, J. Liu, Z. L. Wang, *Science* **2007**, *316*, 102.
[7] J. H. Song, J. Zhou, Z. L. Wang, *Nano Lett.* **2006**, *6*, 1656.
[8] J. Zhou, L. Gong, S. Z. Deng, J. Chen, J. C. She, N. S. Xu, R. Yang, Z. L. Wang, *Appl. Phys. Lett.* **2005**, *87*, 223 108.
[9] J. C. She, S. An, S. Z. Deng, J. Chen, Z. M. Xiao, J. Zhou, N. S. Xu, *Appl. Phys. Lett.* **2007**, *90*, 073 103.
[10] C. Liu, Z. Hu, Q. Wu, X. Z. Wang, Y. Chen, H. Sang, J. M. Zhu, S. Z. Deng, N. S. Xu, *J. Am. Chem. Soc.* **2005**, *127*, 1318.
[11] T.-S. Kang, A. P. Smith, B. E. Taylor, M. F. Durstock, *Nano Lett.* **2009**, *9*, 601.
[12] J. Chen, N. Y. Huang, S. Z. Deng, J. C. She, N. S. Xu, W. Zhang, X. Wen, S. Yang, *Appl. Phys. Lett.* **2005**, *86*, 151 107.
[13] Z. Y. Zhang, K. Yao, Y. Liu, C. H. Jin, X. L. Liang, Q. Chen, L. M. Peng, *Adv. Mater.* **2007**, *17*, 2478.
[14] F. A. Padovani, R. Stratton, *Solid-State Electron.* **1966**, *9*, 695.
[15] Y. Gu, E. S. Kwak, J. L. Lensch, J. E. Allen, T. W. Odom, L. J. Lauholna, *Appl. Phys. Lett.* **2005**, *87*, 047 111.
[16] J. Appenzeller, M. Radosavlijevic, J. Knoch, P. Avouris, *Phys. Rev. Lett.* **2004**, *92*, 048 301.
[17] X. D. Bai, E. G. Wang, P. X. Gao, Z. L. Wang, *Nano Lett.* **2003**, *3*, 1147.
[18] C. H. Lee, J. S. Wang, V. K. Kayatsha, J. Y. Huang, Y. K. Yap, *Nanotechnology* **2008**, *19*, 455 605.
[19] J. S. Wang, V. K. Kayastha, Y. K. Yap, Z. Y. Fan, J. G. Lu, Z. W. Pan, I. N. Ivanov, A. A. Puretzky, D. B. Geohegan, *Nano Lett.* **2005**, *5*, 2528.
[20] C. H. Lee, M. Xie, V. Kayastha, J. S. Wang, Y. K. Yap, *Chem. Mater.* **2010**, *22*, 1782.
[21] X. D. Bai, J. D. Guo, J. Yu, E. G. Wang, J. Yuan, W. Zhuo, *Appl. Phys. Lett.* **2000**, *76*, 2624.
[22] W. L. Wang, X. D. Bai, K. H. Liu, Z. Xu, D. Golberg, Y. Bando, E. G. Wang, *J. Am. Chem. Soc.* **2006**, *128*, 5530.
[23] J. Yu, E. G. Wang, G. C. Xu, *Chem. Phys. Lett.* **1998**, *292*, 531.
[24] F. Liu, J. F. Tian, L. H. Bao, T. Z. Yang, C. M. Shen, X. Y. Lai, Z. M. Xiao, W. G. Xie, S. Z. Deng, J. Chen, J. C. She, N. S. Xu, H. J. Gao, *Adv. Mater.* **2008**, *20*, 2609.
[25] X. J. Wang, J. F. Tian, T. Z. Yang, L. H. Bao, C. Hui, F. Liu, C. M. Shen, C. Z. Gu, N. S. Xu, H. J. Gao, *Adv. Mater.* **2007**, *19*, 4480.
[26] S. S. Fan, M. G. Chapline, N. R. Franklin, T. W. Tombler, A. M. Cassell, H. J. Dai, *Science* **1999**, *283*, 512.
[27] F. Y. Cao, K. F. Zhong, A. M. Gao, C. L. Chen, Q. X. Li, Q. W. Chen, *J. Phys. Chem. B* **2007**, *111*, 1724.

[28] Y. Zhang, N. W. Franklin, R. J. Chen, H. J. Dai, *Chem. Phys. Lett.* **2000**, *331*, 35.
[29] R. H. Fowler, L. W. Nordheim, *Proc. R. Soc. London Ser. A* **1928**, *119*, 173.
[30] H. E. Tomaschke, D. Alpert, *J. Appl. Phys.* **1967**, *38*, 881.
[31] R. V. Latham, N. S. Xu, *High Voltage Vacuum Insulation* (Ed: R. Latham), Academic Press, London, UK **1995**.
[32] J. G. Simmons, *Phys. Rev. Lett.* **1967**, *22*, 657.
[33] J. G. Simmons, *Phys. Rev.* **1968**, *166*, 912.
[34] N. S. Xu, R. V. Latham, in *High-Voltage Vacuum Insulation: Basic Concepts and Technological Practice* (Ed: R. V. Latham), Academic Press, London, UK **1995**, p. 176.
[35] Z. Xu, X. D. Bai, E. G. Wang, Z. L. Wang, *Appl. Phys. Lett.* **2005**, *87*, 163 106.
[36] D. L. Carroll, P. Redlich, P. M. Ajayan, J. C. Charlier, X. Blasé, A. D. Vita, R. Car, *Phys. Rev. Lett.* **1997**, *78*, 2811.
[37] J. M. Bonard, K. A. Dean, B. F. Coll, C. Klinke, *Phys. Rev. Lett.* **2002**, *89*, 197 602.
[38] A. Buldum, J. P. Lu, *Phys. Rev. Lett.* **2003**, *91*, 236 801.
[39] X. Zheng, G. H. Chen, Z. B. Li, S. Z. Deng, N. S. Xu, *Phys. Rev. Lett.* **2004**, *92*, 106 803.
[40] J. Luo, L. M. Peng, Z. Q. Xue, J. L. Wu, *Phys. Rev. Lett.* **2002**, *66*, 155 407.
[41] G. Zhou, W. H. Duan, B. L. Gu, *Phys. Rev. Lett.* **2001**, *87*, 095 504.
[42] F. Liu, P. J. Cao, H. R. Zhang, C. M. Shen, Z. Wang, J. Q. Li, H. J. Gao, *J. Cryst. Growth* **2005**, *274*, 126.
[43] P. J. Cao, Y. S. Gu, H. W. Liu, F. Shen, Y. G. Wang, Q. F. Zhang, J. L. Wu, H. J. Gao, *J. Mater. Res.* **2003**, *18*, 16.
[44] H. T. Yang, C. M. Shen, Y. K. Su, T. Z. Yang, H. J. Gao, Y. G. Wang, *Appl. Phys. Lett.* **2003**, *82*, 4729.
[45] S. T. He, J. N. Yao, P. Jiang, D. X. Shi, H. X. Zhang, S. S. Xie, S. J. Pang, H. J. Gao, *Langmuir* **2001**, *17*, 1571.